Investigation of Solid Lubrication Processes of DLC Films with a Unique 6 Axes UHV Tribometer

Antoine Normant, Jules Galipaud, Frédéric Dubreuil, Julien Fontaine

Tribology Online

Japanese Society of Tribologists
https://www.tribology.jp/trol/

Vol. 18, No. 5 (2023) 239-248.
ISSN 1881-2198
DOI 10.2474/trol.18.239

Article

Investigation of Solid Lubrication Processes of DLC Films with a Unique 6 Axes UHV Tribometer

Antoine Normant [1)], Jules Galipaud [2, 3)], Frédéric Dubreuil [1)] and Julien Fontaine [2)*]

[1)] Univ Lyon, Ecole Centrale de Lyon, CNRS, ENTPE,
Laboratoire de Tribologie et Dynamique des Systèmes (LTDS) UMR5513, 69130 Ecully, France
[2)] Univ Lyon, CNRS, Ecole Centrale de Lyon, ENTPE,
Laboratoire de Tribologie et Dynamique des Systèmes (LTDS) UMR5513, 69130 Ecully, France
[3)] Univ Lyon, CNRS, Institut National des Sciences Appliquées de Lyon,
MATEIS, UMR5510, 69100 Villeurbanne, France

*Corresponding author: Julien Fontaine (julien.fontaine@ec-lyon.fr)

Manuscript received 26 March 2023; accepted 01 June 2023; published 31 August 2023
Presented at the 7th World Tribology Congress 2022 Lyon, July 2022

Abstract

Among Diamond-Like Carbon (DLC) materials, hydrogenated amorphous carbon (a-C:H) coatings may exhibit super-low friction coefficients (< 0.01) under vacuum. A running-in phase is observed in the first few cycles of sliding before reaching a steady state of super-low friction. In this study, a unique ultra-high vacuum tribometer, with 4 different axes of motions and a 6 axes force sensor, is used to characterize the tribological behavior of a steel pin / a-C:H coated flat contact. An original crossing-tracks method is proposed to dissociate the respective roles of tribofilm build-up and surface modifications on the a-C:H in the achievement of super-low friction. A previously build-up tribofilm on the steel counterface shortens the running-in phase by 18 cycles and reduces the initial friction coefficient by 32%. Sliding on a previously rubbed area of the coating allows an additional initial friction reduction of 36%. Morphological and chemical investigations on the a-C:H coated flat using Atomic Force Microscopy and X-ray Photoelectron Spectroscopy reveal that the initial nanoasperities were smoothed, eventually leading to shallow matter transfers and tribofilm thickening on the counterface. Carbon-to-carbon bonds rupture and a reorganization in the carbon structure leads to an increase of the sp^2/sp^3 hybridization ratio.

Keywords

diamond-like carbon, hydrogenated amorphous carbon, super-low friction, ultra-high vacuum, 6 axes force sensor, tribofilm, nano-roughness, carbon hybridization

1 Introduction

Diamond-Like carbon (DLC) thin films present great performances in a wide range of coating applications thanks to their high hardness, wear resistance, chemical inertness and low friction behavior even for dry sliding applications. Those characteristics have raised interests in many industrial fields and led to a large number of studies over the last 30 years [1, 2].

DLC properties are strongly related to their composition and structure, which depend on deposition conditions [1]. In dry sliding experiments, their friction and wear performances are also influenced by the environment. Depending on coating compositions, some DLCs present various tribological performances in inert environments or in presence of reactive species such as hydrogen, oxygen or water vapor [3]. In tribological experiments involving hydrogenated amorphous carbon (a-C:H) films, the friction coefficient increases with increasing relative humidity [4], whereas in experiments involving pure amorphous carbon films, it decreases with increasing relative humidity [5]. Ambient hydrogen favors long life expectancy and low friction [6] unlike ambient oxygen [4].

Among DLC coatings, hydrogenated amorphous carbon (a-C:H) films present great tribological performances under vacuum or inert environments, with reported friction coefficients below 0.01 for steel/a-C:H contacts [7, 8], a regime known as “super-low friction”. In order to obtain such super-low friction, the coating has to be highly hydrogenated. The existence of a threshold in hydrogen content, strongly dependent on the deposition process, has been demonstrated [9]. Hydrogen-to-carbon bonds ensure inertness of the surface

and thus prevent adhesive behavior [6, 10]. Although super-low friction can be achieved with hydrogenated DLC coatings, a running-in phase, with higher initial friction followed by a progressive decrease, is necessary before reaching a steady-state phase of low friction. During sliding experiments, the formation of a tribochemical film or tribofilm is observed on the counterpart along with mild wear of the coating [11-13]. Rehybridization of carbon from sp^3 to sp^2 during tribological experiments has also been reported in experimental as well as numerical studies [10, 14-16].

Friction coefficients in the millirange are arduous to measure and need very accurate sensors to get a reasonable signal to noise ratio. Sadly, information on the precision of sensors and computing methodology for the friction coefficient are rarely presented in the literature. Moreover, misalignment of sensors is of a paramount importance in the error made for such low friction coefficients [17] and single axis sensors, which are generally used, can't avoid this issue.

A specific tribometer equipped with a high resolution 6 axes force sensor [18] has been developed at the Laboratory of Tribology and Dynamics of Systems (LTDS) of Ecole Centrale de Lyon, allowing to measure super-low friction under controlled environments. Thanks to this unique device, this study presents an original method to investigate the respective roles of the growth of the tribofilm and the chemical and morphological modifications occurring on the coating surface. This will provide a better understanding of the phenomena involved in the achievement of super-low friction with hydrogenated DLC films under ultra-high vacuum.

2 Materials and methods

2.1 Materials

The a-C:H samples used in this study, labeled "AC5" in previous works [6, 8, 19], were deposited on 500 µm thick monocrystalline (100) silicon substrate by DC plasma-enhanced chemical vapor deposition under 26 Pa of C_2H_2 with a bias voltage of −500 V. Details on the deposition process are presented by Grill et al. [20]. Hemispherical pins were made of 52100 bearing steel with a curvature radius of 8 mm and were mirror polished. All samples have been ultrasonically cleaned for 5 minutes in 3 successive solvents (heptane, acetone and isopropanol). The coated flats are fixed on 3 mm thick aluminum plates with ultra-high vacuum compliant epoxy adhesive for mounting purpose.

2.2 Tribological and chemical characterizations

The experiments were conducted inside the Environment Controlled Analytical Tribometer (ECAT) of LTDS. This unique device, presented on Fig. 1, consists in several vacuum chambers connected together.

Samples are introduced thanks to a load-lock chamber with a reduced volume, reaching a high vacuum target in the range of 10^{-5} Pa within 15 minutes. A radial distribution chamber is dedicated to the handling of samples, allowing the storage and the transfer of samples between experimental chambers. A first experimental chamber is dedicated to environment controlled tribological experiments (details in section 2.2.1). Another experimental chamber is dedicated to surface analyses (details in section 2.2.3). A last chamber (not used in this study) is dedicated to sample preparation: RF magnetron sputtering coating deposition, large area ion beam etching, gas adsorption with quartz crystal microbalance. All chambers are individually

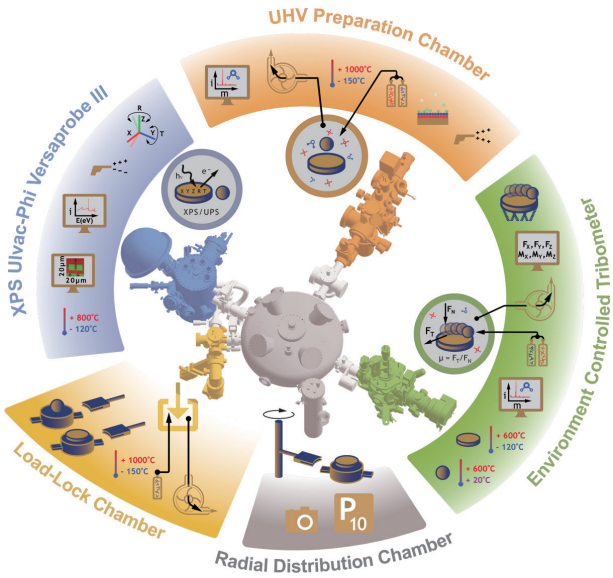

Fig. 1 Schematic presentation of the Environment Control Analytical Tribometer

maintained under ultra-high vacuum, which allows the transfer of samples without any atmospheric contaminations, while allowing independent environment control.

2.2.1 Description of the tribometer

In order to measure super-low friction coefficients ($\mu < 0.01$) inside a vacuum chamber, the use of regular uniaxial sensors raises the issue of the necessary alignment and precision constraints. Any misalignment between the sensors and the forces they are intended to measure can quickly introduce errors of the same order or greater than the friction coefficient [17]. Perfect alignment is practically impossible, especially under vacuum conditions, where the actuators are necessarily far away from the contact under motion. In a previous UHV tribometer [21], this was dealt with transmission of the forces through two shafts, with a high stiffness in the direction of the force to measure but a large compliance in lateral directions, resulting in a low stiffness tribometer. Here, in order to avoid such issue, a 6 axes force sensor is used to measure forces in all directions and take misalignments into account, while preserving a high stiffness of the system.

Under vacuum environment, reduced volume chambers impose the use of compact samples. Balls used in tribological experiments under vacuum are typically millimetric. Thus, conducting experiments with contact pressures of several hundreds of megapascals leads to normal forces in the newton range. Therefore, detecting super-low friction regime imposes accurate measurement of lateral forces in the millinewton range. Commercial 6 axes sensors barely reach this precision and they are not compatible with vacuum environments.

This is why a specific 6 axes force sensor (3 forces and 3 torques) has been developed at LTDS. Its materials are vacuum compliant and its design and components have been chosen to provide a force resolution of at least 1 mN. Under a normal force of 10 N it is thus theoretically possible to measure friction coefficients with a resolution of 10^{-4}. Such performances make it a unique device opening a completely new field of possibilities in term of tribological experiments under environments usually challenging for force measurements. Further information,

detailed design and application examples can be found in a previous article devoted to this unique sensor [18].

This sensor is placed inside the tribometer chamber and is equipped with a receiving dock for the sample holder. To perform tribological experiments, a counter-body on another sample holder is mounted upside down on a manipulator facing the sensor, allowing 4 movements: translation in X, Y and Z directions and rotation R_z around Z axis.

A motor paired with a mechanical transmission allows displacements in the Z direction. During tribological experiments, the normal force is applied using this motor in a range from 0.1 to 10 N. Due to samples misalignments and/or wear, this force may evolve during sliding. To keep the normal force as close as possible to the setpoint, a set of 3 piezoelectric actuators (100 μm range) adjusts the upper sample's Z position in real time using a PID-controlled feedback loop.

Three other motors ensure in-plane displacements (translations along X and Y axes and rotation around Z axis). Those displacements allow relative positioning of the samples as well as tribological experiments between the two counterparts.

Tribological experiments can be conducted under controlled gas pressure from 10^{-7} Pa to the atmospheric pressure inside the tribometer chamber. Any gaseous species may be used as far as it is not harmful to the equipment. For temperature dependent studies, the samples can be heated up or cooled down in a temperature range of −120 to 600°C.

2.2.2 Tribological parameters and data treatment

Unless specified otherwise, the experiments presented here consisted in 2 mm long linear reciprocating strokes at a sliding speed of 1 mm/s under a normal force of 5 N (maximal theoretical Hertzian pressure of 550 MPa). Thanks to the 6 axes sensor and the 4 movements manipulator, any horizontal direction may be used.

The 3 forces and 3 torques were acquired at 2 kHz and their average values were computed for each pass. A cut-off is applied on each pass to remove the irrelevant data measured during the speed inversion between each pass. The friction coefficient μ is defined as the ratio of the tangential force to the normal force and a cycle is defined as the succession of a forward pass and a backward pass. Thanks to the measurement of the forces in X, Y and Z directions, the computation of the actual tangential force is possible, by considering the tangential force vectors in the (X, Y) plane during forward and reverse motion [18], therefore accounting for misalignments issues. Along with the versatile manipulator, it allows to measure friction in any horizontal sliding direction.

Since data are recorded at a frequency of 2 kHz, a single pass contains about 4000 measurement points for a 2 mm long stroke at 1 mm/s sliding velocity. It allows thus the computation not only of a mean friction coefficient or a mean normal force for each pass, but also their standard deviation.

The results may be traditionally plotted as the evolution of the average coefficient of friction with the number of cycles. Nevertheless, spatial information on friction is then lost. A plotting technique, called "triboscopy" [22], is useful to follow local evolution of the friction. It consists in plotting the friction coefficient both as a function of number of cycles and position along the track, its values represented with a color-scale. Here, the horizontal axis stands for the position of the pin along the sliding track, the vertical axis stands for the number of passes. This representation allows to follow the evolution of the friction coefficient in position and time all along the experiment, in one simple diagram.

2.2.3 Chemical surface analysis

Chemical surface analyses were conducted using a PHI VersaProbe III X-ray photoelectron spectroscope (XPS) inside the analysis chamber. The X-ray source is emitting a monochromatized Al K_α radiation (h_ν = 1486.6 eV), its spot size was set at 100 μm. The spectra were collected at 13 eV constant pass energy. Quantification was performed using relative sensitivity factors extracted from a study by Wagner et al. [23] including cross section and escape depth correction, a further angular distribution correction was applied using a source to analyzer angle of 45°.

Those analyses were carried out on the a-C:H coating in order to investigate the potential evolution of sp^2/sp^3 carbon hybridization ratio. Indeed, according to the literature [24], information on sp^2/sp^3 ratio of carbon can be obtained by measuring the binding energy difference between the global maximum and the global minimum of the first derivative of the X-ray excited Auger Electron spectrum (XAES), referenced as "D-parameter". A linear relation between the D-parameter and sp^2/sp^3 ratio has been proposed [25] from 13 eV for diamond (100% sp^3) [26] to 23.1 eV for Highly Oriented Pyrolytic Graphite (HOPG) (100% sp^2) [27]. The derivative spectra were obtained through fitting of the XAES signal. After inelastic background removal through a Shirley-type function, the signal was fitted using 16 components of gaussian-lorentzian line shape. They were all constrained to the same area and full width at half maximum to obtain a converging fit. The overall envelope was then derived to obtain the first derivative XAES spectra. More details on this deconvolution method are presented in a study by Fairley et al. [28]. This technique considerably reduces the noise of the derivative signal, and provides a reliable measurement of the D-parameter. XPS analyzes also allow to determine atomic composition of the surface. Yet, it is essential to mention that hydrogen can't be quantified using XPS.

In this study, chemical characterizations on the pin couldn't be achieved due to the size of the steel pin holder preventing its transfer inside the analysis chamber.

2.3 Morphological characterizations

In addition to tribological and chemical characterizations, morphological characterizations of the samples were conducted outside the vacuum system.

Optical observations of the tracks were conducted using a Keyence VHX-6000 digital microscope in axial-exposure mode with VH-Z100R optics. Brightness and contrast of the pictures have been adjusted in order to increase visibility of the wear tracks, which presented very mild wear.

Scanning Electron Microscopy (SEM) has also been used to study small scale morphology of the wear tracks. Micrographs were obtained using a TESCAN MIRA3 Field Emission Gun SEM in Secondary Emission detection mode with a working distance of 10 mm, an accelerating voltage of 7 kV, an absorbed current of 135 pA and a spot size of 5 nm.

Quantitative measurements of the sample roughness were performed using an atomic force microscope (AFM) Park NX10 in tapping mode. Aluminum coated silicon probe was used on a cantilever with a resonant frequency of 174 kHz and a stiffness in 20-95 N/m range.

3 Results and discussion

3.1 Tribometer performance

The evolution of the friction coefficient and the PID-controlled normal force for a typical experiment of 500 cycles (1000 passes) are presented on Fig. 2. The friction coefficient (orange curve) is plotted in logarithmic scale (each point is the average value for one pass) with its standard deviation for each pass in light orange. The measured normal force is plotted in blue (each point is the average value for one pass) with its standard deviation for each pass in light blue.

The average measurement of the normal force was 4.95 N for forward passes and 5.05 N for backward passes, this is only a 1% deviation from the 5 N target normal force. The maximum recorded standard deviation of the normal force along one pass was 0.5%. Such a low deviation from target normal force and a low variability of this force over each pass demonstrates the efficiency of the tribometer's sensor and load system.

The evolution of the coefficient of friction reveals a "running-in" phase before reaching a super-low friction regime. After an increase from 0.28 to 0.34 during the first 10 cycles, the coefficient of friction drops quickly down to 0.02 at 40 cycles. It slowly decreases then and reach about 0.006 at the end of the experiment, which corresponds to super-low friction.

The evolutions of the friction coefficient over passes #578 and #1000 of this experiment are presented on Fig. 3. The average value of the friction coefficient is the same for those two passes: 5.6×10^{-3}, but the curves are not the same. In order to ensure that the slight differences in these evolutions are indeed originating from tribological phenomena, it is necessary to confirm that they don't originate from measurement noise. In this experiment, with a normal force set to 5 N, the sensor's force resolution of 1 mN allows to measure friction coefficients with a theoretical precision of 2×10^{-4}, which implies an uncertainty of 3.6% at a friction coefficient of 5.6×10^{-3}. The standard deviation of the friction coefficient, over the 4000 measured points, is 4.6% for pass #578 and 11.1% for pass #1000. The standard deviations

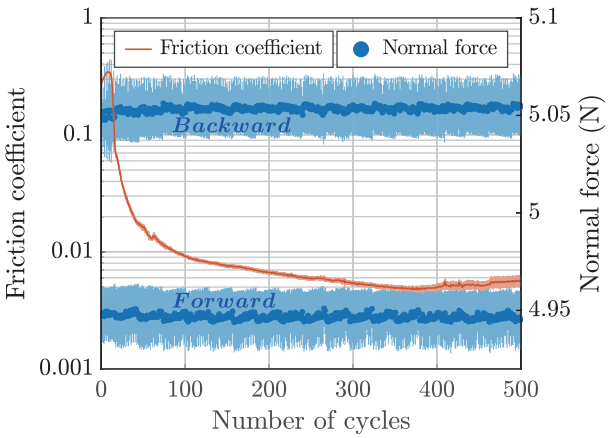

Fig. 2 Evolution of the friction coefficient (orange) and the normal force (blue) for a steel/AC5 contact. The standard deviation of the friction coefficient (light orange) and the normal force (light blue) are also plotted. For normal force measurements, data are split in two groups, which correspond to forward and backward passes. Note the logarithmic scale for the friction coefficient.

are greater than the measurement uncertainty. Therefore, the measured variations of the friction coefficient over a pass don't originate from the tribometer but reveals actual heterogeneities in the tribological behavior, which seem to evolve during the sliding experiment. Pass #578 presents a more homogeneous friction than pass #1000 for which higher variations are visible on track's ends. The resolution of the 6 axes sensor along with the performances of the active load system demonstrate this tribometer ability to measure super-low friction ($\mu < 0.01$).

The evolution of the friction coefficient during the running-in phase suggests that the sliding interface is evolving, with some modifications of the rubbed surfaces. Optical observations of the pin wear scar and the flat wear track after 500 cycles indeed reveal few shallow grooves on the coating as well as a tribofilm formation on the pin (Fig. 4). As can be seen on those images, the localization of the grooves on the flat matches the localization of thick tribofilm patches on the pin: the wear induced on the coating contributes to the thickening of the tribofilm.

3.2 Respective roles of the tribofilm and the coating surface modifications

To better understand the phenomena leading to the reduction of friction, it is necessary to dissociate the respective

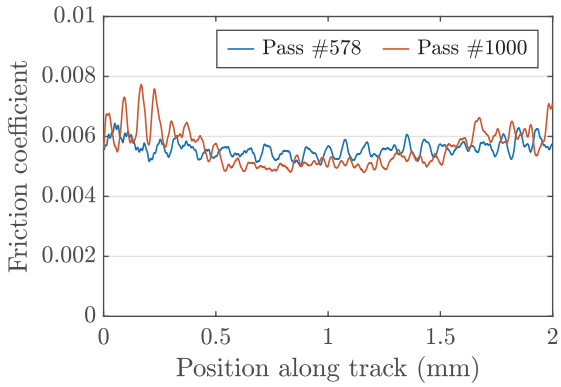

Fig. 3 Evolution of the friction coefficient for a steel/AC5 contact along two selected passes presenting the same average friction coefficient over the pass (pass #578 in blue and pass #1000 in orange)

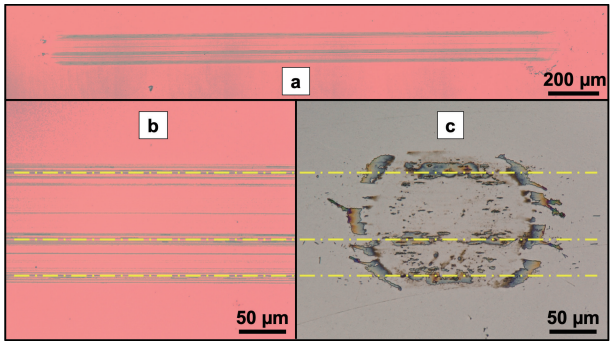

Fig. 4 Optical observations of the rubbed surfaces. General view of the wear track on the a-C:H coated flat (a), detail of a part of the track (b) and wear scar on the pin (c). Yellow dotted lines are plotted in (b) and (c) to highlight the correspondence between thicker tribofilm on the pin and shallow grooves on the flat.

roles of the modifications on the pin, with the growth of a tribofilm, and on the flat, with wear. To achieve this, specific experiments have to be designed:

- To explore the role of the tribofilm, a previously rubbed area of the pin, with already formed tribofilm, may be rubbed against a fresh, unworn area of the a-C:H coated flat.
- To explore the role of modifications on the coating, the evolution of the friction coefficient across worn and unworn areas of the a-C:H coated flat may be observed.

The presence of already formed tribofilm on the pin or previous modifications on the flat should affect the evolution of the friction coefficient.

Thanks to the unique design of the tribometer, with 6 axes force sensor and 4 axes displacements, it is possible to perform sliding experiments in any horizontal direction. 5 reciprocal sliding tests were performed with experimental conditions listed in Table 1. The pattern of the experiments can be seen on the optical observation of Fig. 5. The first 3 sliding tracks are parallel, the fourth experiment was conducted perpendicularly, crossing the three previous tracks, and the fifth test is crossing all previous tracks with a 45° angle. This fifth track was produced in order to illustrate the versatile possibilities of displacements inside the tribometer.

When crossing a previous wear track, it is possible to compare the friction coefficient along a pass in worn and unworn areas of the coating within a single experiment. Figure 6 (a) presents the evolution of the friction coefficient versus the position inside track #4 for few selected passes. The triboscopical representation of the experiment is also presented on Fig. 6 (b). Right from the first passes, the friction coefficient is lowered whenever the pin crosses a previous track. With

Table 1 Experimental parameters for 5 crossing tracks

#	*Initial tribofilm*	*Load*	*Length*	*Cycles*	*Orientation*
1	No	3 N	2 mm	500	0°
2	Yes	5 N	2 mm	500	0°
3	Yes	5 N	2 mm	1000	0°
4	Yes	5 N	2 mm	500	90°
5	Yes	5 N	3 mm	500	45°

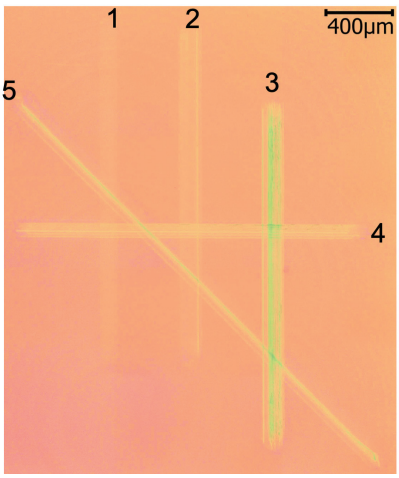

Fig. 5 Optical observation of 5 crossing tracks on the a-C:H coated flat

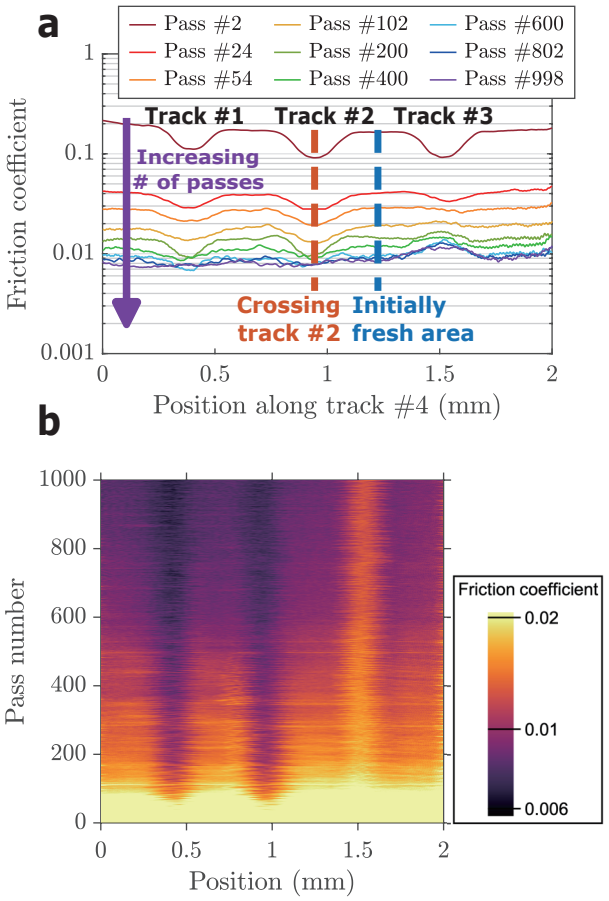

Fig. 6 Evolution of the friction coefficient along track #4 for selected passes (a) and corresponding triboscopical image (b). Note the logarithmic scale for the friction coefficient.

increasing number of passes, the coefficient of friction decreases for every position along the track, with lower values in initially worn areas.

Only for higher number of passes a slight local increase in friction (< 0.004) can be observed when crossing track #3. On the optical observation of Fig. 5 color variations on the coating allows to see the tracks. Tracks #1 and #2 present a homogeneous slightly lighter color than on unrubbed areas. No grooves are visible, contrary to track #3. Test #3 was performed for 1000 cycles, versus 500 cycles for tracks #1 and #2. Therefore, wear must be more pronounced in this track. Slightly higher friction when crossing track #3 might be due to the presence of those grooves.

Figure 7 presents the evolution of the friction coefficient over the first 30 cycles in 3 different conditions. Curve A corresponds to an experiment conducted elsewhere on a fresh area of the a-C:H coated flat with a fresh steel pin surface. Curves B and C are both extracted from test #4, for which the pin surface has already undergone friction and a tribofilm is present on its surface. Two different positions inside the track are compared, curve B corresponding to an initially fresh area and curve C corresponding to the crossing of the previous track #2, as shown by dashed lines on Fig. 6 (a). Therefore, 3 conditions are presented: no tribofilm against unworn area on the coating in a first experiment (curve A) and already grown tribofilm against unworn areas (curve B) and worn areas

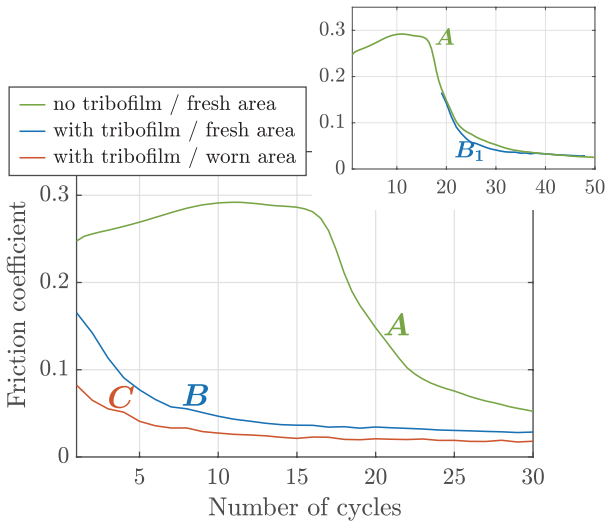

Fig. 7 Evolution of the friction coefficient under 3 particular conditions for the first 30 cycles. Curve A (green) corresponds to an experiment on a fresh area of the a-C:H film with a fresh steel pin surface. Curves B (blue) and C (orange) are both extracted from test #4 at two different positions inside the track: in an initially fresh area of the flat (B) and crossing track #2 (C). On the inset of this figure, curve B is plotted with an offset of 18 cycles and is labelled as "B_1".

(curve C) of the coating in a single second experiment. In this experiment, comparing these 3 curves allows to discuss the respective roles of the tribofilm build-up on the steel ball and the wear on the a-C:H coated flat on the establishment of super-low friction.

Curve A shows a running-in phase, with an increase of the friction coefficient from 0.25 to 0.29 during the first 15 cycles, followed by a sharp decrease. Such tribological behavior has already been observed for steel/a-C:H contacts [13]. When sliding a previously rubbed pin surface against a fresh area of the a-C:H coated flat, this running-in phase is altered: curve B exhibits a lower initial value of the friction coefficient of 0.17 (instead of 0.25) and a monotonous decrease of the friction coefficient from the beginning of the experiment. When sliding the same previously rubbed pin surface against a previously worn area of the flat, the running-in phase is further altered: curve C reveals an initial friction coefficient lowered to 0.08, the trend being unchanged, with a monotonous decrease of the friction coefficient.

Curve B_1 presented on the inset of Fig. 7 corresponds to curve B plotted with an offset of 18 cycles. Curve B_1 almost perfectly overlaps curve A: the presence of a previously build-up tribofilm allows to start the experiment inside the friction drop phase as if 18 cycles were skipped. Thus, the running-in phase is shortened thanks to the previously build-up tribofilm on the steel counterface. In a study by McClimon et al. [29] using colloidal steel probes as counterface of an a-C:H coating in an atomic force microscope, experiments showed that, during the friction rising phase of the running-in, the probe height had not significantly increased. On the contrary, the probe height rose quickly after the beginning of the friction drop. Therefore, either no more than barely measurable atomic layers of the tribofilm appeared during the high friction phase, or the wear of the coating is compensated by the growth of the tribofilm, which can be not only vertical but also lateral. The tribofilm starts to thicken faster than the coating is wearing out during the friction drop phase. According to this study, the thickening of the tribofilm in the present experiments may then start during the friction drop phase.

Those results show that both the tribofilm build-up and previous rubbing on the coating affect the way low friction is reached. A thick tribofilm takes some time to form (between 15 and 30 cycles) and leads to a drastic reduction in friction (here 32% reduction at the beginning of the experiment). But the modifications on the coating also favors low friction achievement (36% supplementary initial friction reduction in this experiment, see Fig. 7, curve C). Understanding the modifications occurring on the a-C:H surface during sliding is therefore paramount to better understand achievement of super-low friction.

3.3 Morphological and chemical investigations on the coating surface

The SEM micrographs of narrow areas on Fig. 8 reveal the morphology of the coating at high magnification (×94000) outside and inside track #3. Outside the track, the coating presents asperities of few tens of nanometers. Those asperities seem to have been flattened inside the wear track. Yet, they are still visible and their height distribution looks more homogeneous. Asperities flattening may induce the slightly lighter color visible inside all the tracks shown on Fig. 5. A

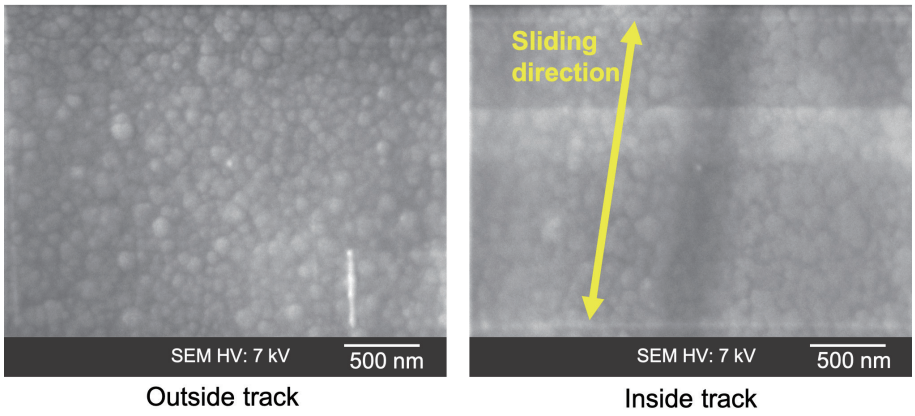

Fig. 8 High magnification SEM observations of narrow areas outside and inside the track #3 on the a-C:H coated flat. The sliding direction is shown in yellow.

shallow groove can also be seen inside track #3. At first, little quantity of matter is transferred at the asperities' scale causing their flattening. This roughness reduction may eventually lead to larger contact areas and slightly deeper matter removal on the coating. This leads to shallow grooves on the flat and formation of tribofilm patches on the counterpart. Those grooves, mainly visible in track #3, which was performed for larger number of passes than tracks #1 and #2, are up to 100 nm deep (10% of the as deposited a-C:H coating's thickness). Although these shallow grooves represent larger wear than nanoscale roughness reduction, they are localized and still constitute mild wear. Using colloidal steel atomic force microscopy probes as the sliding counterface, McClimon et al. [29] presented tribological experiments where the initially high friction first increased without an important tribofilm build-up, then the effective contact area has been shown to increase quickly along with a rapid thickening of the tribofilm. Those results are consistent with a prior roughness reduction before the thickening of the tribofilm due to adhesive wear.

Figure 9 presents AFM measurements conducted outside and inside track #3 on 5×5 µm areas to quantify the roughness modification on the coating. Outside the wear track, asperities up to 15 nm high and a few tens of nanometers wide can be observed. As observed by SEM, the asperities are still present inside the track on AFM measurements. Nevertheless, the roughness is significantly reduced from S_a = 2 nm outside the track to S_a = 0.5 nm inside the track. The height distribution, presented on Fig. 10, confirms a far more uniform morphology after sliding, as well as the extracted profile of Fig. 11.

A 2 mm long friction experiment was performed for 675 cycles in order to investigate the chemical modifications (XAES/XPS) of the a-C:H surface along the sliding. XPS allows near surface chemical analyses (2-6 nm), therefore the tiniest pollution on the surface can affect the results. Moreover, surface contaminations mainly consist in organic compounds. Since the a-C:H coating is composed of carbon and hydrogen, the presence of hydrocarbons on the surface can easily affect the analyses. In order to reduce this interference, the first 5 cycles of the experiment were performed over a track length of 2.5 mm, which is then decreased to 2 mm for the remainder of the experiment. The amount of organic compound in the 0.5 mm added part of the track should be reduced, without affecting too much the a-C:H surface. In the following part, this area was taken as the reference state of unrubbed a-C:H coating.

After this experiment, the sample is transferred under UHV to the surface analysis chamber, without exposure to the atmosphere. Chemical compositions obtained by XPS in analyzed areas are listed in Table 2, revealing that only carbon and oxygen could be found on the surface. The overall quantity of oxygen recorded by XPS drops from 14 at.% on the pristine coating to 9 at.% after 5 cycles and to 6 at.% after 675 cycles. This suggests that oxygen belongs mainly to contaminants on the surface of the coating and is progressively removed

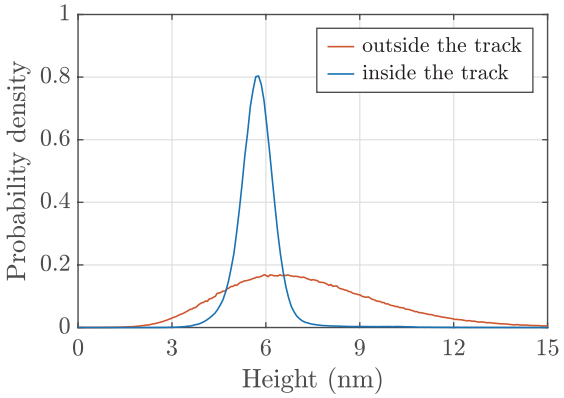

Fig. 10 Height distribution outside (orange) and inside the track #3 (blue) on the a-C:H coated flat

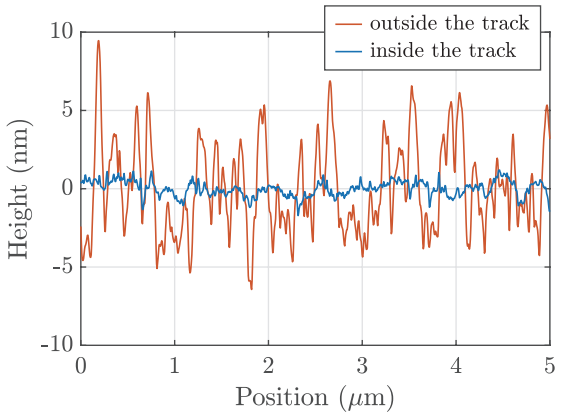

Fig. 11 Profile extracted from the AFM measurements outside (orange) and inside the track #3 (blue) on the a-C:H coated flat

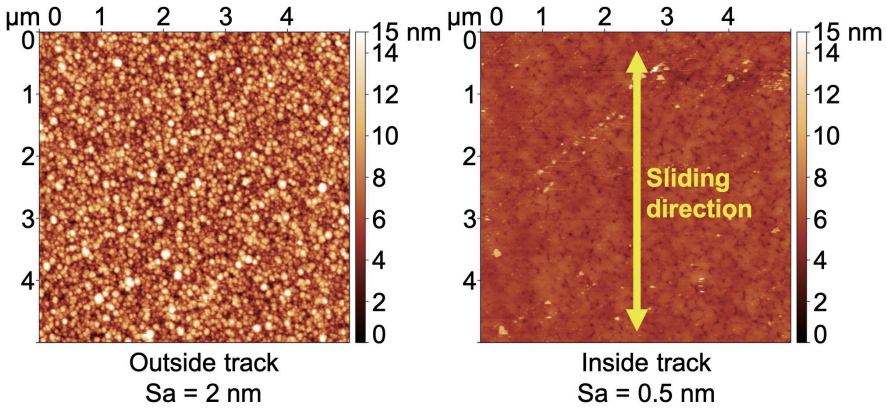

Fig. 9 5 x 5 µm AFM measurements outside the track and inside the track #3 on the a-C:H coated flat. The sliding direction is shown in yellow.

Table 2 Chemical compositions obtained by XPS analyses on different areas of the a-C:H coated flat (hydrogen not considered)

Element	*Outside track*	*5 cycles*	*675 cycles*
Carbon (C1s)	86%	91%	94%
Oxygen (O1s)	14%	9%	6%
Iron (Fe2p)	/	No evidence	No evidence

from the surface. Moreover, no evidence of iron was found by XPS, confirming that no transfer from the pin has happened during friction, oxygen can't be associated with iron oxide build-up on the surface. XAES analyses were performed in order to investigate whether the sp^2/sp^3 carbon ratio of the coating has been modified during the sliding experiment. The first derivative XAES spectra after 5 cycles and after 675 cycles are presented on Fig. 12. On those spectra an evolution of the D-parameter from 13.9 eV to 16.6 eV can be measured, which points toward an increase of the sp^2/sp^3 hybridization of carbon in the film after friction. Evolution of the D-parameter has been initially ascribed to a direct evolution of the sp^2/sp^3 ratio [25], however careful studies on a-C:H coatings show that an evolution of the D-parameter is also correlated with the quantity of oxygen in the film [30]. In this work of Calliari et al., a decrease from 20 to 10 at.% of oxygen in the a-C:H film leads to an increase from 14 to 16.5 of the D-parameter. In the results presented here, the oxygen content evolution is much smaller (9 to 6 at.%) and the big increase in D-parameter doesn't seem to be solely explained by oxygen amount decrease. However, it demonstrates that extreme care must be taken in the interpretation of D-parameter evolution. Moreover, although sp^2/sp^3 carbon ratio seems to increase after sliding, in this study, its evaluation was only conducted at the beginning and at the end of the experiment. It is thus hazardous to link this evolution to super-low friction achievement. Indeed, purely sp^2 materials such as graphite are known to exhibit very high friction coefficients under vacuum [31]. The evolution of the sp^2/sp^3 ratio observed here is clearly a consequence of wear, but there is no evidence of its potential role on friction reduction.

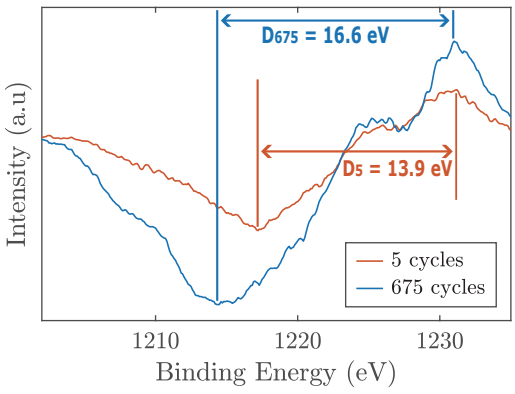

Fig. 12 Derivative XAES spectra inside a 5 cycles area (orange) and a 675 cycles area (blue) of a wear track on the a-C:H coated flat. Measurements of the D-parameter are shown.

The breaking of nanoscale adhesive junctions causes nanoasperities' wear on the coating and matter transfer on the counterface to form the tribofilm. The rupture of carbon-to-carbon bonds should leave dangling bonds. Therefore, the coating's surface becomes highly reactive. As the present experiment was conducted under ultra-high vacuum, there is no environment to react with in order to passivate the surface. The most probable path to avoid such dangling bonds is for the carbon structure to reorganize and thus modify the sp^2/sp^3 carbon ratio. Indeed, even though hydrogen might come out of the coating due to its degradation, a study by Mangolini [16] has showed that in order to completely avoid rehybridization of the carbon during sliding experiments, 2 bar of hydrogen gas was needed.

The experiments presented above reveal that the wear of the initial asperities on the a-C:H surface leads to a reorganization in the carbon structure with rise of the sp^2/sp^3 ratio. SEM and AFM showed that those asperities are a few tens of nanometers wide. XPS/XAES analyzes were conducted on 100 µm wide areas, therefore the results are averaged on millions of those asperities. As shown in Table 2, 6 at.% of oxygen remained present in analyzed areas of the track. As the asperities still exist after sliding, it is possible that hollows between those asperities did not take part in the contact and therefore remained pristine and covered with organic contamination. Identically, XAES analyzes are averaged on areas composed of several asperities and hollows.

Asperities wear causes overall roughness reduction. Thus, larger junctions may form and adhesive wear responsible for shallow matter transfer on the counterpart may occur. Where this transfer from the coating occur, the tribofilm thickens on the facing locations of the counterpart. When sliding with a previously build-up tribofilm on an unworn area of the coating, the initial friction coefficient is lowered and the running-in phase is altered: the friction coefficient monotonously decreases from first cycle on. In this situation, the initial contact is no longer steel on a-C:H but carbonaceous film on a-C:H. Thus, either adhesive junctions between the tribofilm and the coating are weaker than between steel and coating, or the tribofilm acts as a solid lubricant with low shear strength [32].

An original tribological experiment conducted with an already grown tribofilm on the steel pin crossing previous tracks exhibits a different friction coefficient inside and outside the previous tracks. From first cycle on, the friction coefficient is lowered whenever the pin crosses the previous tracks, as seen on the triboscopical representation of Fig. 6 (b). Therefore, wear on the coating favors a reduction in friction. This demonstrates that both the tribofilm formation on the pin and modifications on the coating favor the achievement of low friction.

4 Conclusions

The lubrication processes involved in the contact between a hydrogenated amorphous carbon coated flat and a steel pin under ultra-high vacuum were investigated with a unique Environment Controlled Analytical Tribometer.

A running-in phase starting with high friction coefficient has been evidenced for all experiments. For a standard experiment, with previously unrubbed surfaces, a slight increase in friction during the first tens of cycles is observed before it significantly decreases to reach super-low friction. The formation of a tribofilm on the pin along with mild wear of the coating have been pointed out. In order to investigate the role

of the tribofilm, an experiment with a previously rubbed steel pin surface was conducted. When sliding against a fresh area of the coating, the running-in phase was altered. Initial friction coefficient was lowered by 32% and the first phase of friction increase disappeared, leaving only a monotonous decrease of the friction coefficient: starting with a carbonaceous/a-C:H contact rather than steel/a-C:H allowed to shorten the running-in phase. When sliding with a previously build-up tribofilm against a worn coating surface, the initial friction coefficient is lowered by an additional 36%. Thus, modifications on the coating surface during sliding also favors the achievement of low friction.

During sliding, the nanoscale roughness of the coating is found to decrease and height distribution becomes homogeneous, which leads to the tribofilm formation and thickening on the steel counterface. Although the initial nanoscale asperities on the a-C:H surface are smoothed, they don't disappear. Asperities' wear implies the rupture of carbon-to-carbon bonds, leaving unstable dangling bonds on the surface. This could lead to carbon rehybridization and explain the sp^2/sp^3 ratio increase observed in the wear tracks. A running-in phase with a monotonous decrease of friction is still observed in all presented experiments. Therefore, other phenomena must also occur during this decrease of friction.

The original 6 axis sensor used in this study has showed its capacity to measure super-low friction coefficients (< 0.01) with a high resolution under ultra-high vacuum. An original method to dissociate the respective roles of surface modifications on the a-C:H coating and tribofilm formation on the steel counterpart has been proposed thanks to the versatile manipulator of the tribometer combined with a 6 axes sensor, allowing together the sliding in any direction on the flat sample. Such original experiments finally permit the use of the tribometer as an analytical device to probe previous tracks.

Acknowledgments

The authors would like to thank the European Union within the framework of the FEDER project of the Auvergne-Rhône-Alpes region, PLATEFORME TRIBOLOGIE MOTEURS, for their financial support for the surface analysis system.

Author contributions

AN conceived and performed the experiments and wrote the manuscript. JG conceived the spectroscopic analyzer setup, helped analyze the data and maintained the ECAT. FD conceived the atomic force microscope setup and helped analyze the data. JF designed the tribometer, conceived and performed the experiments and supervised AN.

References

[1] Robertson J. Diamond-like amorphous carbon. Materials Science and Engineering: R: Reports. 2002;37(4–6): 129-281.

[2] Yu Q, Chen X, Zhang C, Luo J. Influence factors on mechanisms of superlubricity in DLC films: a review. Frontiers in Mechanical Engineering. 2020;6: 65.

[3] Donnet C, Erdemir A. Tribology of diamond-like carbon films. Springer. New York. 2008: 155-200.

[4] Donnet C, Le Mogne T, Ponsonnet L, Belin M, Grill A, Patel V, Jahnes C. The respective role of oxygen and water vapor on the tribology of hydrogenated diamond-like carbon coatings. Tribology Letters. 1998;4: 259-265.

[5] Voevodin AA, Phelps AW, Zabinski JS, Donley MS. Friction induced phase transformation of pulsed laser deposited diamond-like carbon. Diamond and Related Materials. 1996;5(11): 1264-1269.

[6] Donnet C, Fontaine J, Grill A, Le Mogn T. The role of hydrogen on the friction mechanism of diamond-like carbon films. Tribology Letters. 2000;9(3-4): 137-142.

[7] Miyake S. Tribological properties of hard carbon films: extremely low friction mechanism of amorphous hydrogenated carbon films and amorphous hydrogenated SiC films in vacuum. Surface and Coatings Technology. 1992;54-55: 563-569.

[8] Donnet C, Grill A. Friction control of diamond-like carbon coatings. Surface and Coatings Technology. 1997;94-95: 456-462.

[9] Fontaine J, Loubet JL, Le Mogne T, Grill A. Superlow friction of diamond-like carbon films: a relation to viscoplastic properties. Tribology Letters. 2004;17(4): 709-714.

[10] Gao GT, Mikulski PT, Harrisson JA. Molecular-scale tribology of amorphous carbon coatings: effects of film thickness, adhesion, and long-range interactions. Journal of the American Chemical Society. 2002;124(24): 7202-7209.

[11] Memming R, Tolle HJ, Wierenga PE. Properties of polymeric layers of hydrogenated amorphous carbon produced by a plasma activated chemical vapour deposition process ii: tribological and mechanical properties. Thin Solid Films. 1986;143: 31-41.

[12] Grill A. Tribology of diamondlike carbon and related materials: an updated review. Surface and Coatings Technology. 1997;94-95: 507-513.

[13] Donnet C, Erdemir A. Tribology of diamond-like carbon films. Springer. New York. 2008: 139-154.

[14] Le Huu T, Zaidi H, Paulmier D, Voumard P. Transformation of sp^3 to sp^2 sites of diamond like carbon coatings during friction in vacuum and under water vapour environment. Thin Solid Films. 1996;290-291: 126-130.

[15] Pastewka L, Moser S, Moseler M. Atomistic insights into the running-in, lubrication, and failure of hydrogenated diamond-like carbon coatings. Tribology Letters. 2010;39: 49-61.

[16] Mangolini F, Koshigan KD, Benthem MHV, Ohlhauson JA, McClimon JB, Hilbert J, Fontaine J, Carpick RW. How hydrogen and oxygen vapor affect the tribochemistry of silicon- and oxygen-containing hydrogenated amorphous carbon under low-friction conditions: a study combining X-ray absorption spectromicroscopy and data science methods. ACS Applied Materials and Interfaces. 2021;13(10): 12610-12621.

[17] Schmitz TL, Action JE, Ziegert JC, Sawyer WG. The difficulty of measuring low friction: uncertainty analysis for friction coefficient measurements. Journal of Tribology. 2005;127(3): 673-678.

[18] Guibert M, Oliver C, Durand T, Le Mogne T, Le Bot A, Dalmas D, Scheibert J, Fontaine J. A versatile flexure-based six-axis force/torque sensor and its application to tribology. Review of Scientific Instruments. 2021;92(8): 085002.

[19] Fontaine J, Le Mogne T, Loubet JL, Belin M. Achieving superlow friction with hydrogenated amorphous carbon: some key requirements. Thin Solid Films. 2005;482(1-2): 99-108.

[20] Grill A, Patel V. Stresses in diamond-like carbon films. Diamond and Related Materials. 1993;2(12): 1519-1524.

[21] Le Mogne T, Martin JM, Grossiord C. Imaging the chemistry of transfer films in the AES/XPS analytical UHV tribotester. Tribology Series. 1999;36: 413-421.

[22] Belin M, Martin JM. Triboscopy, a new approach to surface degradations of thin films. Wear. 1992;156(1): 151-160.

[23] Wagner CD, Davis LE, Zeller MV, Taylor JA, Raymond RH, Gale LH. Empirical atomic sensitivity factors for quantitative analysis by electron spectroscopy for chemical analysis. Surface and Interface

Analyses. 1981;3(5): 211-225.

[24] Mizokawa Y, Miyasato T, Nakamura S, Geib KM, Wilmsen CW. Comparison of the CKLL first-derivative auger spectra from XPS and AES using diamond, graphite, SiC and diamond-like-carbon films. Surface Science. 1987;182(3): 431-438.

[25] Lascovitch JC, Scaglione S. Comparison among XAES, PELS and XPS techniques for evaluation of sp^2 percentage in a-C:H. Applied Surface Science. 1994;78(1): 17-23.

[26] Lurie PG, Wilson JM. The diamond surface: ii. secondary electron emission. Surface Science. 1977;65(2): 476-498.

[27] Lesiak B, Zemek J, Houdkova J, Kromka A, Jozwik A. Electron spectra line shape analysis of highly oriented pyrolytic graphite and nanocrystalline diamond. Analytical Sciences. 2010;26(2): 217-222.

[28] Fairley N, Compagnini G, Scardaci V, Baltrus J, Roberts A, Barlow A, Cumpson P, Baltrusaitis J. Surface analysis insight note: differentiation methods applicable to noisy data for determination of sp^2- versus sp^3-hybridization of carbon allotropes and AES signal strengths. Surface and Interface Analysis. 2023;55(3): 165-175.

[29] McClimon JB, Hilbert J, Koshigan KD, Fontaine J, Lukes JR, Carpick RW. In situ growth and characterization of lubricious carbon-based films using colloidal probe microscopy. Tribology Letters. 2023;71: 39.

[30] Calliari L, Filippi M, Gottardi G, Laidani N, Anderle M. An electron spectroscopy study of a-C:H films produced by PACVD in a CH_4–CO_2 gas mixture. Surface Science. 2005;586(1-3): 96-108.

[31] Bryant PJ, Gutshall PL, Taylor LH. A study of mechanisms of graphite friction and wear. Wear. 1964;7(1): 118-126.

[32] Erdemir A, Eryilmaz O. Achieving superlubricity in DLC films by controlling bulk, surface, and tribochemistry. Friction. 2014;2: 140-155.